J. Fluid Mech. (2006), *vol.* 548, *pp.* 1–16.
doi:10.1017/S0022112005007378 Printed in the United Kingdom

Mean flow structure in thermal convection in a cylindrical cell of aspect ratio one half

By G. STRINGANO AND R. VERZICCO

Politecnico di Bari, DIMeG and CEMeC, Via Re David 200, 70125 Bari, Italia

(Received 3 May 2005 and in revised form 21 July 2005)

In this paper we propose a simple model that, by comparing different time scales, allows a prediction for the mean flow structure and its dynamics in confined thermal convection in a cylindrical cell of aspect ratio (diameter over cell height) $\Gamma = 1/2$. It is shown that the break-up of the mean elongated recirculation into two counter-rotating unity-aspect-ratio rolls, sometimes referred to as flow bimodality, occurs only in a narrow range of Rayleigh numbers whose extrema depend on the Prandtl number. The predictions of the present model are consistent with the published literature, according to which the dual mean flow structure has been observed in numerical simulations at $Pr = 0.7$ and experiments in gaseous helium ($Pr \approx 0.7$) but never in water at 'ambient' temperature ($Pr \approx 5$) and only once in water at $T = 80\,^{\circ}\mathrm{C}$ ($Pr = 2$). Another prediction of the model is that the thermal properties of the sidewall affect the mean flow unsteadiness and, sometimes, prevent transitions via a subtle anchoring mechanism that has been identified and verified by *ad hoc* numerical simulations.

1. Introduction

The long-term dynamics of thermally driven flows have recently attracted renewed interest owing to their implications for meteorological (reversal of constant winds) and geophysical (inversion of the Earth's magnetic field) applications as well as in the interpretation of some experimental measurements. It has been observed, in particular, that the large-scale recirculation of a confined thermally driven flow remains relatively stable in position and magnitude for hundreds or even thousands of large-eddy turnover times and then suddenly experiences an abrupt reversal which occurs in a time of the order of one large-eddy turnover time. An interpretation of the causes, dynamics and statistics of the flow reversals has been given by Sreenivasan, Bershadskii & Niemela (2002) and Araujo, Grossmann & Lohse (2005). These papers considered a cylindrical cell of aspect ratio (diameter over cell height) $\Gamma = 1$ since the mean flow consists of a circular unity-aspect-ratio roll completely filling the cell. While for this configuration the structure of the mean flow and how it behaves are relatively clear, much less is known for an equally popular geometry: the cylindrical cell of aspect ratio $\Gamma = 1/2$. In particular, in this slender cell some numerical simulations (Verzicco & Camussi 2003) and experiments (Roche *et al.* 2002) have found, respectively, two possible mean flow configurations and a flow bimodality evidenced by two equally probable Nusselt number values for the same Rayleigh number. However, these experiments and numerical simulations were all at Prandtl number $Pr \approx 0.7$ or higher while recent experiments performed in the same geometry but in water at strictly constant Prandtl number ($Pr \approx 5$) did not show any transition and the mean flow consisted only of a stable single roll completely filling

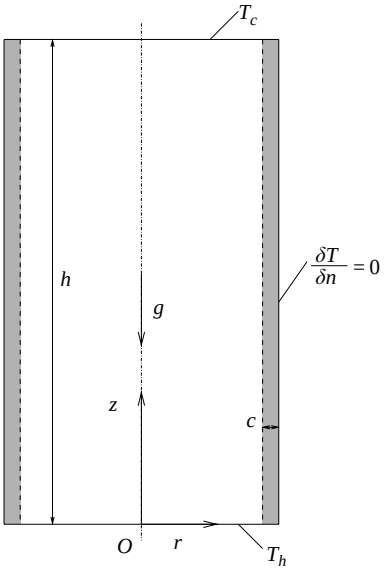

FIGURE 1. Sketch of the cell (vertical plane cut).

the cell (Nikolaenko *et al.* 2005; Sun, Xi & Xia 2005). On the other hand, in a recent experiment (Chillà *et al.* 2004) performed in a large cell with water at $T = 80\,^{\circ}\mathrm{C}$ ($Pr \approx 2$), indications of flow bimodality have been reported. Within this scenario, some experimentalists 'deliberately do not use an aspect ratio close to $\Gamma = 1/2$ in an effort to avoid the multi-stability' mean flow structure (Brown *et al.* 2005*b*).

In the present paper we argue that a combination of Rayleigh and Prandtl number effects and sidewall thermal properties are the cause of the observed differences. We present simple theoretical arguments for the proposed explanation that will allow a consistent reinterpretation of the published literature. We will then show the results of numerical simulations that confirm the theoretical expectations. The paper is closed by a discussion of some controversial results for the mean flow structure (Verzicco & Camussi 2003; Roche *et al.* 2002; Nikolaenko *et al.* 2005; Sun *et al.* 2005) and for heat transfer measurements (Chavanne *et al.* 2001; Niemela *et al.* 2000) whose differences can be explained in the light of the present model.

2. Problem and numerical setup

In this paper we numerically simulate the flow developing in a cylindrical cell vertically confined by flat plates, the lower being hotter than the upper (respectively at temperatures T_h and T_c). The flow is bounded laterally by a sidewall of thickness c and with thermal properties (denoted by subscript w) which are different from those of the fluid (denoted by subscript f). The lateral wall is no-slip and continuity of temperature and heat flux is assumed at the interface between fluid and solid. At the 'dry' surface of the sidewall adiabatic conditions are imposed (figure 1). The numerical code is the same as in Verzicco (2002) where details of the numerical method and validation tests are described. In short, we solve the Navier–Stokes equations with the Boussinesq approximation:

$$\frac{\mathrm{D}\,\boldsymbol{u}}{\mathrm{D}\,t} = -\boldsymbol{\nabla} p + \theta \hat{\boldsymbol{z}} + \left(\frac{Pr}{Ra}\right)^{1/2} \boldsymbol{\nabla}^2 \boldsymbol{u}, \qquad \boldsymbol{\nabla}\cdot\boldsymbol{u} = 0 \quad \text{on} \quad V_f,$$

$$\frac{\mathrm{D}\theta}{\mathrm{D}t} = \frac{1}{(PrRa)^{1/2}} \frac{\rho_f C_{pf}}{\rho C} \nabla \cdot \left(\frac{\lambda}{\lambda_f} \nabla \theta \right) \quad \text{on} \quad V,$$

with V_f the volume occupied only by the fluid, V the volume of fluid and sidewall, ρ_f, C_{pf} and λ_f with $k_f = \lambda_f/(\rho_f C_{pf})$, respectively, density, constant-pressure specific heat and thermal conductivity of the fluid and ρ, C and λ the same quantities for the fluid or the solid (ρ_w C_w and λ_w) depending on the point in the domain; $\hat{\boldsymbol{z}}$ is the axial unity vector pointing in the opposite direction to gravity, $\boldsymbol{u}$ the velocity vector, p the pressure and θ the non-dimensional temperature. The equations have been made non-dimensional using the free-fall velocity $U = \sqrt{g\alpha_f \Delta h}$, the distance between hot and cold plates h and their temperature difference $\Delta = T_h - T_c$; therefore the Rayleigh and Prandtl numbers are, respectively, $Ra = g\alpha_f \Delta h^3/(\nu_f k_f)$ and $Pr = \nu_f/k_f$ with g the acceleration due to gravity, α_f the isobaric thermal expansion coefficient, ν_f the kinematic viscosity and k_f the thermal diffusivity of the fluid. The non-dimensional temperature θ is defined $\theta = (T - T_c)/\Delta$ so that $0 \leqslant \theta \leqslant 1$.

The above equations have been written in a cylindrical coordinate frame and discretized on a staggered mesh by central second-order accurate finite-difference approximations. For every simulation the mesh size was chosen in such a way that it was of the order of the Kolmogorov scale in the bulk of the flow and that the thinnest of the viscous and thermal boundary layers was resolved at least by 6 gridpoints. This yielded grids ranging from $33 \times 33 \times 129$ up to $129 \times 97 \times 385$ nodes in the azimuthal radial and axial directions, depending on Ra and Pr, which according to Grötzbach (1983) provided enough spatial resolution to properly resolve the flow field. Some additional simulations discussed are those by Verzicco & Camussi (2003) where all the convergence checks have been performed.

3. Results

In order to better explain our arguments we will briefly describe the flow configurations of figure 2, showing perspective views of temperature isosurfaces for various Rayleigh numbers at $Pr = 0.7$. When the Rayleigh number is small (figure 2*a*) the flow is smooth and with reduced fluctuations; thus the single-cell large-scale flow produces a stable vertical ascending hot current on one side and a descending cold current on the opposite side. The thickness of each current is of the same order as the thermal boundary layer thickness δ_θ. Hereafter, for the sake of brevity we will always refer to the warm ascending current generated at the lower hot plate even if, for symmetry reasons, the same arguments would apply also to the cold descending stream generated at the upper plate. During the ascending motion the warm current loses heat owing to diffusion and, as we will see later, whether the hot fluid reaches the upper cold plate depends on the vertical velocity of the current and on its thickness.

As the Rayleigh number is increased the thermal boundary layer thickness decreases and so does the thickness of the vertical currents. In addition, in agreement with the observations of Qiu & Tong (2001), the amplitude of the velocity fluctuations becomes comparable to that of the mean flow, thus perturbing the stability of the structures. This is evident in figure 2(*b*) where the vertical currents appear convoluted and irregular. If the Rayleigh number is further augmented there is the possibility that the hot side current becomes so thin and convoluted that it loses all its excess heat with respect to the ambient fluid before reaching the upper plate. Should this happen the current cannot rise up to the upper plate and it must sink somewhere in between to regain heat from the lower plate: when this occurs the single recirculation splits into

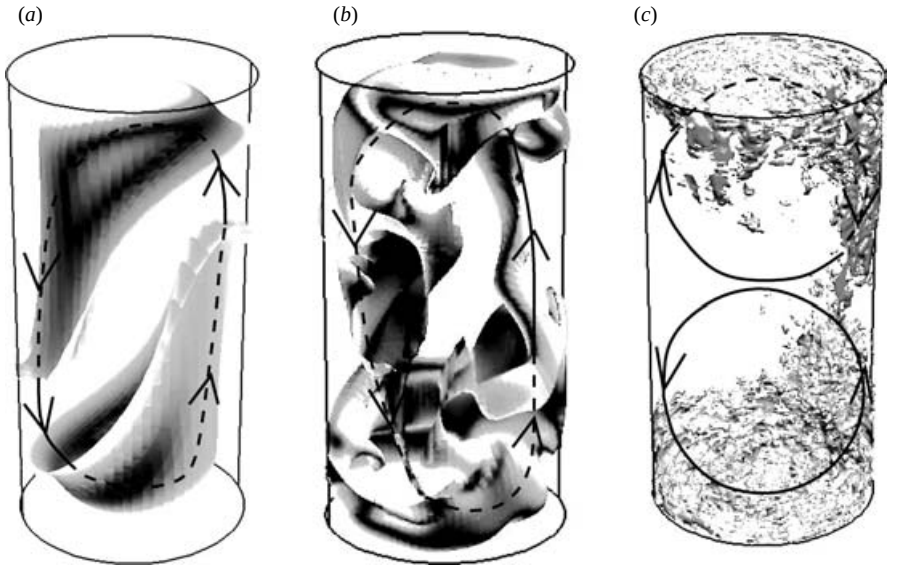

FIGURE 2. Perspective views of temperature isosurfaces at $Pr = 0.7$: (*a*) $Ra = 6 \times 10^5$, (*b*) $Ra = 2 \times 10^8$, (*c*) $Ra = 2 \times 10^{10}$. Light grey $T = 0.6\Delta$, dark grey $T = 0.4\Delta$.

two cells as shown in figure 2(*c*) where hot and cold side currents are on the same side of the cell and they only exist for half the plate separation distance h.

Of course these dynamics and the occurrence of the different possibilities depend on the Rayleigh and Prandtl numbers since both the ascending velocity of the current and its thickness depend on these parameters. In order to make quantitative observations on figure 2 we refer to the sketch of figure 3(*a*) showing the warm current having a thickness ℓ equal to the thermal boundary layer δ_θ and rising with a velocity U. If h is the distance from plate to plate, the time taken for a fluid particle inside the current to travel that distance is $t_U \approx h/U$ while the time the same particle needs to lose its excess heat with respect to the ambient fluid can be estimated as the diffusive time $t_f \approx \ell^2/k_f \approx \delta_\theta^2/k_f$. If however the rising current has to cross the whole cell height it must remain buoyant during the ascent implying that $t_U/t_f < 1$. If we estimate the velocity U as the free-fall velocity $U \approx \sqrt{g\alpha_f \Delta h}$ and the thermal boundary layer thickness as $\delta_\theta/h \approx 1/(2Nu)$ we obtain $t_U/t_f \approx 4Nu^2/(RaPr)^{1/2}$ which can be used for quantitative estimates once the appropriate correlation for $Nu = Nu(Ra, Pr)$ is assumed. A possible flaw in the proposed model is the assumption that the diffusion time determines the heat dynamics inside the ascending current since in a turbulent flow the effective diffusion is enhanced with respect to the molecular value.

It must be noted, however, that in this particular geometry the vertical currents are produced by vortex-ring-like recirculations attached to the bottom and top plates that stretch the boundary layers radially outward at the plates and convect them vertically along the sidewall where the flow is at most transitional. This prevents most of the plumes from being released at the centre of the plates and evolving in the bulk where the flow is turbulent. The situation would be completely different in a large-aspect-ratio domain or in a rectangular tank like that in Puthenveettil & Arakeri (2005) where the thermal plumes merge together and organize themselves into thick structures, most of the vertical motion is within the bulk, and the turbulent diffusion certainly governs the dynamics. In addition, if $\delta_\theta/h \approx 1/(2Nu)$ and $\eta/h \sim [Pr^2/(RaNu)]^{1/4}$ with $Nu \sim Ra^\beta$

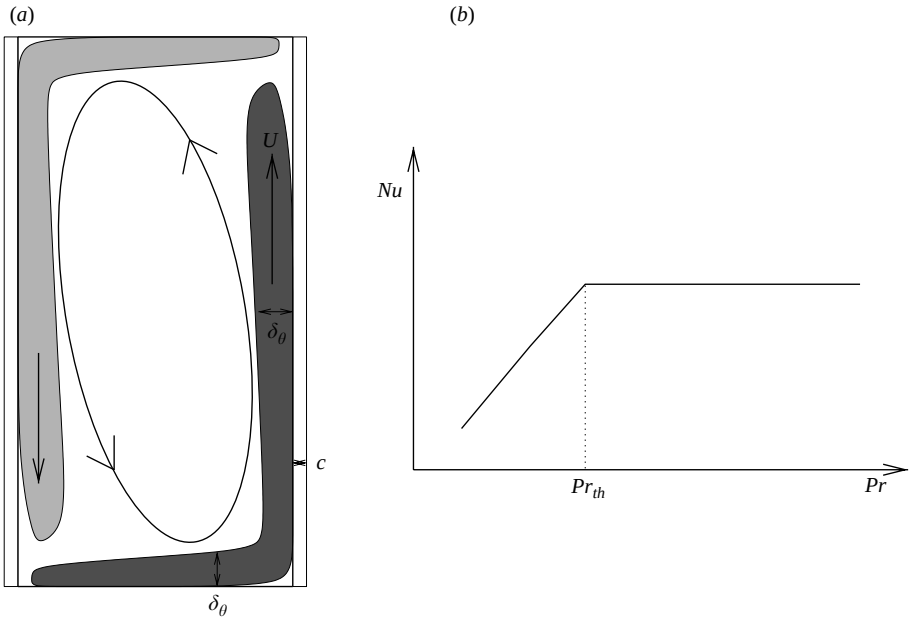

FIGURE 3. (*a*) Sketch of the side currents arrangement, (*b*) sketch of the Nusselt number dependence on the Prandtl number for a constant Rayleigh number.

then $\delta_\theta \sim Ra^{-\beta}$ and $\eta \sim Ra^{-(1+\beta)/4}$. For $\beta = 1/3$ which is approximately correct, at least for $Pr \geqslant 0.7$, the two exponents match, implying that η and δ_θ decrease at the same rate with the Rayleigh number. This is confirmed by Verzicco & Camussi (2003) who report the values $\eta/h = 0.0185$, $\delta_\theta/h = 0.0163$ at $Ra = 2 \times 10^7$, $\eta/h = 0.0039$, $\delta_\theta/h = 0.0050$ at $Ra = 2 \times 10^9$ and $\eta/h = 0.0010$, $\delta_\theta/h = 0.0011$ at $Ra = 2 \times 10^{11}$. Since η and δ_θ are always of the same order we have in the $\Gamma = 1/2$ cell that the thickness of the ascending current is in the dissipative range and it is indeed governed by molecular diffusion. We note, in passing, that this argument would hold even if the side current were thicker since η is known to underestimate the size of the dissipative motion by a factor two (Pope 2000) and the energy dissipation peaks at a scale of about 10η (Monin & Yaglom 1975). At a speculative level we can also argue that even if two or more plumes indeed merged together to form a thicker structure they should diffuse into each other. This brings us back to the diffusive time t_f, meaning, in other words, that while merging together the plumes also lose heat to the ambient fluid and the present model could remain valid.

Another point deserving further discussion is the assumption that the vertical velocity of the side current is of the order of the free-fall velocity. In fact as noted by Niemela *et al.* (2001) and Verzicco & Camussi (2003), respectively for cylindrical cells of aspect ratio $\Gamma = 1$ and $\Gamma = 1/2$, the mean circulation velocity is only a fraction of U (of the order of 20 %–50 %) and this could be accounted in the model by a numerical factor C ($U' \approx C\sqrt{g\alpha_f \Delta h}$). It is however also true that in order for a single recirculation to be formed the vertical current does not need to be buoyant along the whole height h since, owing to continuity, a neutrally buoyant part of the current above a buoyant one would be pushed up anyway. Also, this phenomenon could be accounted by a numerical coefficient that presumably would compensate (at least in part) the previous one. This consideration, together with the desire to maintain the

model free from tunable parameters, lead us to use all the arguments in their simplest version and to test the resulting crude model against the experimental results.

According to the available literature (see for example Grossmann & Lohse 2001, 2002) it is clear that the relation between Nu, Ra and Pr is not a simple power law and in addition the cell aspect ratio and even its shape play non-negligible roles. A common feature is however that the Nusselt number increases monotonically with the Rayleigh number while it increases with the Prandtl number up to a threshold value and then saturates as sketched in figure 3(b). It should be stressed that the real $Nu(Ra, Pr)$ behaviour is more complex since, as shown by Grossmann & Lohse (2001) the position of the knee and the slope of the inclined part of the Nu vs. Pr curve depends on the Rayleigh number while the horizontal part should have a small decrease for very large Pr which is also Ra dependent. Nevertheless, for the sake of simplicity, we will assume a correlation $Nu = ARa^{\beta}$ for $Pr \geqslant Pr_{th}$ and $Nu = BPr^{\gamma}Ra^{\beta}$ for $Pr < Pr_{th}$ keeping in mind that β, γ and Pr_{th} might possibly depend on Ra and Pr if all the curvatures of the $Nu(Ra, Pr)$ relation have to be retained as suggested by Grossmann & Lohse (2001). The above correlation for $Pr \geqslant Pr_{th}$ inserted in the estimate for t_U/t_f yields

$$\frac{t_U}{t_f} = \frac{4A^2Ra^{2\beta}}{(RaPr)^{1/2}}, \tag{3.1}$$

which gives $t_U/t_f > 1$ for either small or large Rayleigh numbers depending on whether the exponent β is smaller or larger than 1/4 respectively. The former case ($\beta < 1/4$) would indicate that the free-fall velocity is small and the ascending time is too long for the current to maintain its heat. The latter case, in contrast, suggests that the current is too thin and its heat is diffused to the ambient fluid before a particle in the current is convected from plate to plate. Experimental and numerical evidence, however, shows that always $\beta > 1/4$ and only the second possibility occurs in reality. This is confirmed by the formation of large-scale circulations at very low Rayleigh numbers after the onset of convection and, in the other extreme, by the difficulty of distinguishing a mean motion from the background fluctuations at high Rayleigh numbers. In the 'low' Prandtl number regime $Pr < Pr_{th}$ similar arguments apply and the appropriate $Nu(Ra, Pr)$ estimate inserted in the t_U/t_f formula gives

$$\frac{t_U}{t_f} = \frac{4B^2Pr^{2\gamma}Ra^{2\beta}}{(RaPr)^{1/2}}. \tag{3.2}$$

Both (3.1) and (3.2) give a ratio t_U/t_f which increases with Ra and eventually crosses the boundary $t_U/t_f = 1$; this determines a threshold Rayleigh number Ra_{th} above which a single recirculation spanning the whole cell height cannot be supported by the system. If however we allow the single elongated cell to split into two unity-aspect-ratio cells, the ascending current will have to travel only a reduced distance $h' = h/2$ which in turn will give a shorter convection time $t'_U = h'/U$, a new ratio t'_U/t_f and an augmented threshold Ra'_{th}. The complete behaviour of the system is summarized in figure 4 where the position of the intersections C and D depends on the values of the various flow (Pr) and correlation (A, B, γ, β) parameters.

In particular, figure 4 suggests that a single elongated roll can be found in the system only up to $Ra = Ra_C$ while the two-rolls mean flow can exist up to $Ra = Ra_D$ and it is the only possible configuration in the range $Ra_C \leqslant Ra \leqslant Ra_D$. Figure 4 implies also that for $Ra \leqslant Ra_C = Ra_{D''}$ both the single cell and the two-rolls configurations are possible and the flow can switch over time from one configuration to another if enough unsteadiness is present. Above the threshold $t_U/t_f = 1$ no mean flow can exist

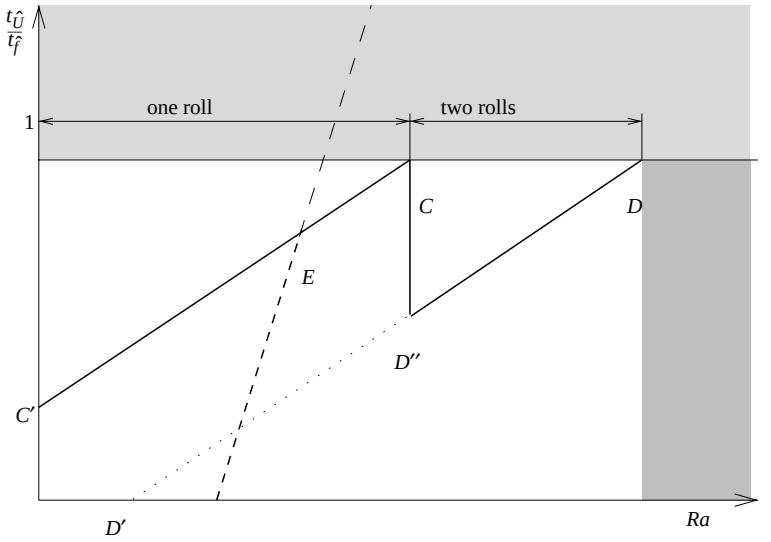

FIGURE 4. Phase diagram for the characterization of the mean flow structure: —— $C'C$, equation (3.1) or (3.2); ····· $D'D''$ and —— $D''D$, equation (3.1) or (3.2) but for the distance $h' = h/2$ instead of h (the segment $D'D''$ shows the region where the two-rolls configuration can be formed as an alternative to the single cell); – – – –, t_w/t_f. In the shaded regions no mean flow is observed. The axes are represented in logarithmic scale.

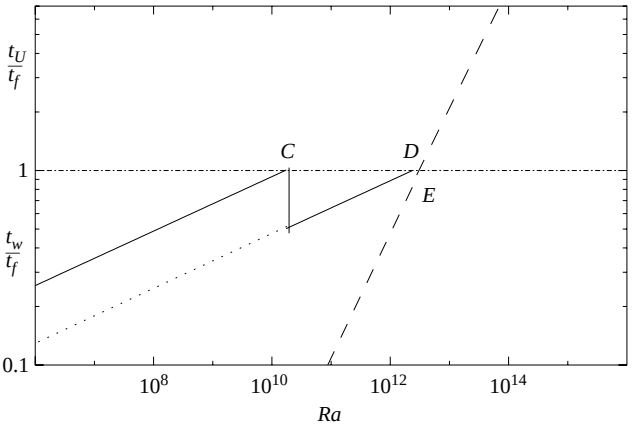

FIGURE 5. Phase diagram for the mean flow structure: —— and ·····, t_U/t_f; – – –, t_w/t_f at $Pr = 0.7$ for gaseous helium/stainless steel and $c/h = 0.0025$; —·—, boundary for $t_U/t_f = 1$. The relation $Nu = 0.088Ra^{0.32}$ has been used to draw the diagram.

since any warm coherent current rising vertically loses its heat to the ambient fluid before it can be significantly convected. Another limit for the existence of a mean flow is $Ra \leqslant Ra_D$, at least until further break-ups (never observed) are introduced.

The prediction of the phase diagram of figure 4 has been tested using some results from the literature; at $Pr = 0.7$ for cryogenic gaseous helium it can be assumed that $Nu \approx 0.088Ra^{0.32}$ (J. Niemela, personal communication) which plugged into (3.1) yields the plot of figure 5. From that figure we have $Ra_C = 1.6 \times 10^{10}$ and $Ra_D = 3.0 \times 10^{12}$

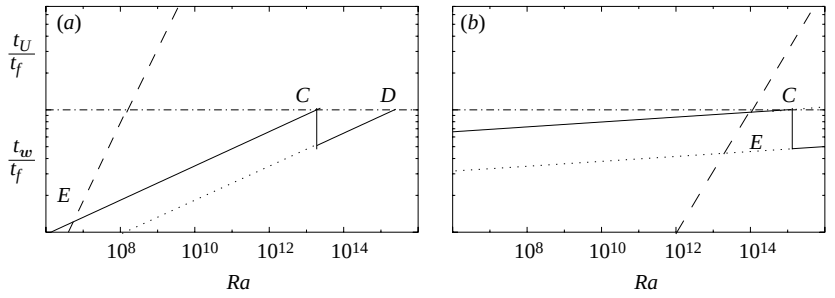

FIGURE 6. The same as figure 5 but for (*a*) $Pr = 5$: ----, water/Plexiglas (with $c/h = 0.0125$ and $Nu = 0.088Ra^{0.32}$). (*b*) $Pr = 0.022$: ----, mercury/stainless steel (with $c/h = 0.005$ and $Nu = 0.251Pr^{0.16}Ra^{0.26}$).

which are consistent with the transitional values observed by Verzicco & Camussi (2003) and with the bimodal flow behaviour described by Roche *et al.* (2002).

The same estimates but for $Pr = 5$ (water) are reported in figure 6(*a*) which gives $Ra_C = 1.9 \times 10^{13}$ and $Ra_D = 3.3 \times 10^{15}$; since experiments in water have never been performed at Rayleigh number above 10^{13} observations and measurements have always shown for the mean flow a single elongated cell (Nikolaenko *et al.* 2005; Sun *et al.* 2005) as predicted by the present model. Although in a slightly different context, some arguments on the different time scales involved in the experiments in water and gaseous helium have been given by Roche *et al.* (2004) where it is also suggested that the double mean flow structure is more difficult to see in water than in helium.

In the low Prandtl number regime, the Nusselt number depends also on the Prandtl number (figure 3*b*) and a fit for the results obtained in liquid metals (Rossby 1969; Cioni, Ciliberto & Sommeria 1997; Horanyi, Krebs & Müller 1999; Verzicco & Camussi 1999) for $Pr \leqslant 0.1$ gives $Nu = 0.251Pr^{0.16}Ra^{0.26}$ which together with equation (3.2) yields the results of figure 6(*b*) for mercury ($Pr = 0.022$). In this case the first intersection occurs at $Ra_C = 9.5 \times 10^{14}$ and the second would be around 10^{30}; this is consistent with the literature where no indications of the two-rolls configuration are reported. It should be stressed, however, that this last result should be taken with caution since, given the reduced slope of the lines for t_U/t_f in figure 6(*b*), small differences in the fit parameters might results in large shifts of the crossings.

Looking at figure 4 we can see that another result of the model is the possibility for the flow to support both the single-roll and the two-rolls configurations for $Ra < Ra_C$. The switching between the two structures will depend on the flow unsteadiness which is likely to produce a vertical ascending current with an inhomogeneous temperature distribution and therefore to trigger the transition. This mechanism is essentially the same as that suggested by Sreenivasan *et al.* (2002) and Araujo *et al.* (2005) in which the flow unsteadiness could produce a thermal plume much hotter or colder than the average and this 'freak' event triggered wind reversal in a cylindrical cell of aspect ratio $\Gamma = 1$. In the present $\Gamma = 1/2$ cylindrical cell it might then happen that part of the ascending current is released from the lower plate at colder than the average temperature and it becomes non-buoyant before reaching the upper plate, thus triggering the transition. However, except for numerical simulations, the sidewall is never perfectly adiabatic and in particular conditions strong temperature inhomogeneities in the ascending current could be damped by the heat stored in the sidewall. Once again we have therefore to compare time scales, which will be $t_f = \delta_\theta^2/k_f$ for the fluid and $t_w = c^2/k_w$ for the wall with c and k_w, respectively, the thickness

and the thermal diffusivity of the sidewall. If $t_w/t_f \gg 1$ the fluid adjusts quickly to the sidewall temperature which, because of its large thermal inertia, tends to stabilize the flow. In contrast, when $t_w/t_f \ll 1$ the current does not feel the thermal effect of the sidewall which, having a small heat capacity, produces a negligible perturbation to the vertical current. The idea that the thermal properties of the sidewall affect the flow unsteadiness is confirmed by the observations of Sreenivasan *et al.* (2002) who observed a change in the statistics of the wind reversals after inserting an insulating layer of mylar over the entire inner surface of the stainless steel sidewall of their experimental setup. By using the same estimates as equation (3.1) we can write

$$\frac{t_w}{t_f} = \left(\frac{c}{h}\right)^2 4A^2 Ra^{2\beta} \frac{k_f}{k_w}, \tag{3.3}$$

reported in figures 4, 5 and 6 as a dashed line (for figure 6(*b*) the estimates of equation (3.2) have been employed); it is important to note that while the slope of the line is determined only by the $Nu(Ra, Pr)$ relation, its position in the plot depends on construction details of the experimental apparatus. The intersection of the curves for t_U/t_f and t_w/t_f (point E) therefore depends on the flow but also on the setup, and it determines the region where $t_w/t_U < 1$ or vice versa. In fact, for a transition in the mean flow structure to be possible not only must the flow unsteadiness not be damped by the sidewall but the latter must not act as an 'anchoring' device for the mean flow. In other words, if a plume were sufficiently not to reverse the flow with an ideal sidewall it could cool down directly by contact with the surface of a real sidewall. However even if the plume were to hit the upper plate with enough heat to reverse the flow the same plume might not be strong enough to reverse the mean flow and at the same time to change the temperature field inside the sidewall. If the sidewall is not to anchor the mean flow, therefore, its temperature must change quickly with respect to the turnover time or $t_w/t_U \ll 1$; in figures 4, 5 and 6 this happens when the Rayleigh number is smaller than Ra_E.

In figures 5 and 6 some examples of the consequences of this prediction are reported for the combinations stainless steel/gaseous helium (figure 5), water/Plexiglas (figure 6*a*) and stainless steel/mercury (figure 6*b*). The model suggests that for the wall thicknesses commonly used in the experiments ($c/h = 0.0025$) a stainless steel sidewall does not perturb the flow unsteadiness in gaseous helium up to $Ra_E \approx 5 \times 10^{12}$, beyond the limit for the existence of a coherent mean flow ($Ra = Ra_D$). The same estimates for water and Plexiglas (with $c/h = 0.0125$), in contrast, yield $Ra_E \approx 10^6$ implying that the unsteady dynamics of the mean flow are practically always influenced by the stabilizing effect of the sidewall. Finally for the mercury and stainless steel, where $c/h = 0.0025$, we find $Ra_E \approx 10^{14}$ which is higher than any experiment performed to date but smaller than Ra_C, thus suggesting possible effects of the sidewall on the mean flow.

Partial confirmation of these predictions has been obtained by *ad hoc* numerical simulations performed with different values of the Prandtl number and sidewall properties. Consider first a perfectly adiabatic sidewall, or a wall with zero thickness $c = 0$ (and zero heat capacity), which therefore cannot perturb the mean flow dynamics ($Ra_E \longrightarrow \infty$). As shown by Oresta, Stringano & Verzicco (2005) the mean flow at $Pr = 0.7$ and $Ra = 9 \times 10^5$ consists preferentially of a single elongated recirculation although it occasionally splits into two counter-rotating rolls that only last few large-eddy turnover times and then immediately disappear to give again a unique structure with a different azimuthal orientation than the original one. This behaviour is shown

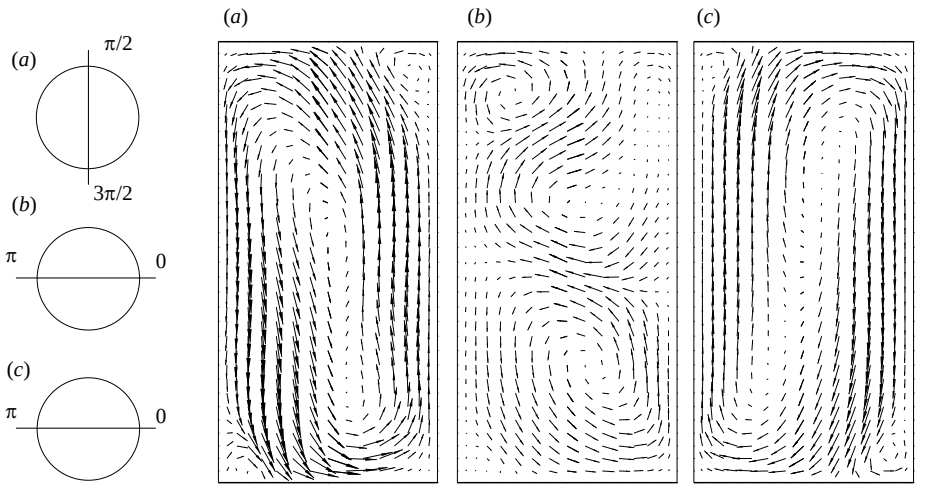

FIGURE 7. Instantaneous vertical sections of velocity vectors across a mean flow transition event, $Ra = 9 \times 10^5$ and $Pr = 0.7$: (*a*) $t = 180$, (*b*) $t = 190$, (*c*) $t = 200$.

by direct flow observations across the transition (compare figure 7 and the arrow in figure 8*a*) and by time series of vertical velocity sampled at a fixed point showing reverse-like features (figure 8*a*). The same simulation performed for the combination of gaseous helium and stainless steel gives the results of figure 8(*b*) with essentially the same dynamics as that of a perfect sidewall. Similar observations have been reported at a higher Rayleigh number by Wu & Libchaber (1992) who state that 'in the $\Gamma = 1/2$ cell the large-scale velocity switches direction from time to time'. A simulation in the same geometry but for water and with a sidewall of Plexiglas of thickness $c/h = 0.0125$ gives the results of figure 8(*c*) indicating the presence essentiall of a stable elongated structure which is consistent with the threshold $Ra_E \approx 10^6$ of figure 6(*a*). Note that the flow of figure 8(*c*) was computed at $Ra = 6 \times 10^6$ that, with the Prandtl number of water, yielded the same Reynolds number $Re = \sqrt{Ra/Pr}$ as that of figure 8(*a*,*b*); the same dynamics, however, has been observed for smaller values of *Ra*.

Brown *et al.* (2005*a*) report that in a $\Gamma = 1$ cylindrical cell filled with water and with a Plexiglas sidewall two kinds of flow reversals can be found, 'cessations' and 're-orientations', the latter being far more probable than the former. In the first case the flow momentarily stops and then reverses the sense of rotation while in the second case it never stops rotating and it simply reorients itself by a slow azimuthal tilting. Comparing the time scale of the single velocity jump of figure 8(*c*) with those in 8(*a*,*b*) it should be evident that the event in figure 8(*c*), being slower, should be a reorientation. On the other hand it should be noted that the present model, concerning the flow dynamics in a vertical meridional plane, can only make predictions for the cessations; therefore the reversal of figure 8(*c*) should not be interpreted as a discrepancy with the proposed model.

Finally for mercury and stainless steel the sidewall should have negligible influence on the mean flow dynamics and the results of figure 8(*d*) confirm the expectation.

It is worth mentioning that the effect of the sidewall conductivity on the flow was investigated by Ahlers (2001), Roche *et al.* (2001*a*), Verzicco (2002), and Niemela & Sreenivasan (2003), but they focused only on a correction to the heat transfer to account for the parasite heat current through the lateral wall. In the present case, the

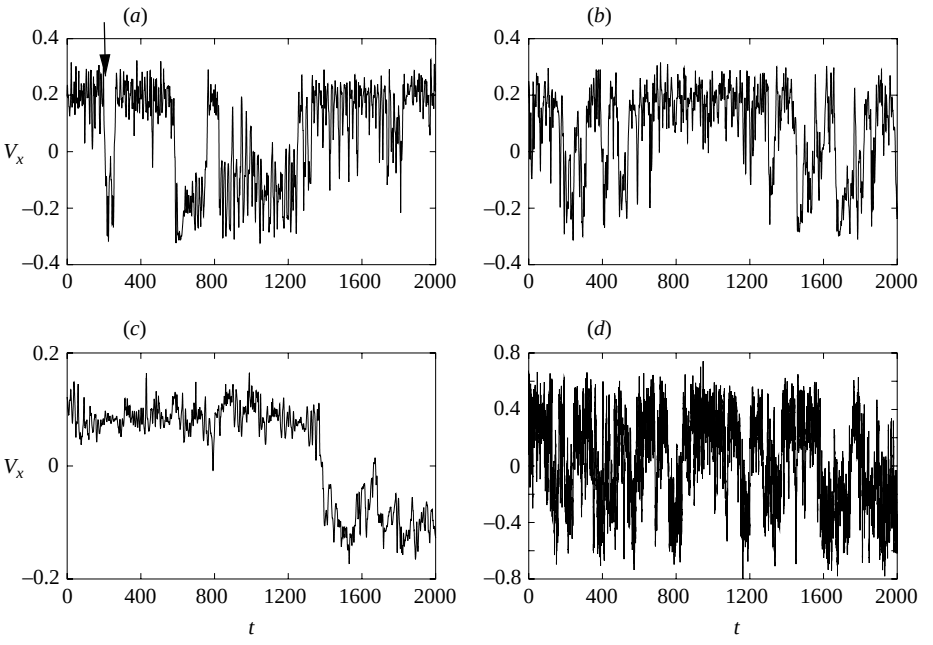

FIGURE 8. Time histories of pointwise samples of vertical velocity at $xh = 0.25$, $r/h = 0.2$ and $\phi = 0$ (axial, radial and azimuthal coordinates). (*a*) $Ra = 9 \times 10^5$ and $Pr = 0.7$, ideal sidewall ($c = 0$); (*b*) $Ra = 9 \times 10^5$ and $Pr = 0.7$, sidewall with $(c/h)^2(k_f/k_w) = 1.28 \times 10^{-6}$ (gaseous helium/stainless steel with a wall thickness $c/h = 0.0025$); (*c*) $Ra = 6 \times 10^6$ and $Pr = 5$, sidewall with $(c/h)^2(k_f/k_w) = 1.91 \times 10^{-4}$ (water/Plexiglas with a wall thickness $c/h = 0.0125$); (*d*) $Ra = 9 \times 10^5$ and $Pr = 0.022$, sidewall with $(c/h)^2(k_f/k_w) = 5.58 \times 10^{-6}$ (mercury/stainless steel with a wall thickness $c/h = 0.0025$). The arrow in (*a*) refers to the time of figure 7.

effect is very different being related to the heat stored in the sidewall and not to the flux through it. We note, by the way, that the present effect is more subtle since it is more important in those configurations where the heat transfer correction would be negligible.

4. Discussion

The relations for t_U/t_f and t_w/t_f with the conditions $t_U/t_f = 1$ and $t_w/t_f = t_U/t_f$ can be used to draw phase diagrams in the (*Ra*, *Pr*)-plane for the mean flow structure and its dynamics. Three representative cases are shown in figures 9–11 with the plane divided into four regions depending on the presence of one single roll (1R) or two rolls (2R) in the mean flow and the unstable (U regions with possible temporary transitions) or stable (S) character of the recirculations. The shaded regions (NMF) of figures 9–11 are those where, according to the model, a mean flow is not formed because thermal plumes are too small or the convection velocity too slow to establish an organized flow.

Superimposed on the diagrams of figures 9–11 we also show the *Ra*–*Pr* values for some experiments performed in a cylindrical cell of aspect ratio $\Gamma = 1/2$. The cryogenic helium experiments (figure 9), because of the particular experimental technique, are not performed at constant *Pr* but one that increases at the highest *Ra*. The data for two recent experiments (Niemela *et al.* 2000; Chavanne *et al.* 2001) are reported in figure 9 and owing to the different size of the cells the *Ra*–*Pr* curves follow different paths.

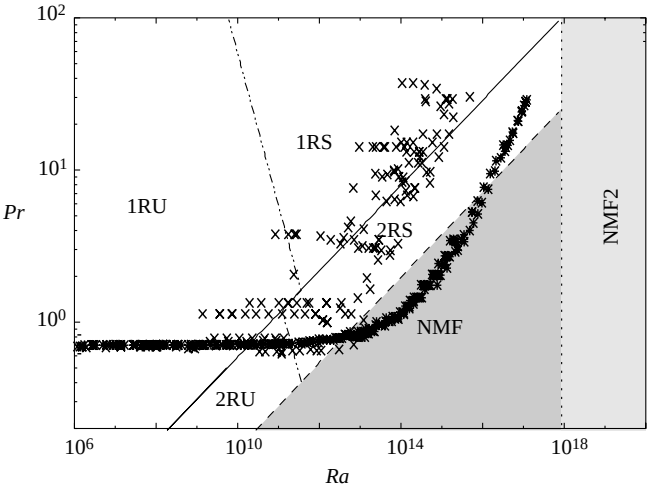

FIGURE 9. Phase diagram for the mean flow structure: regions 1R* indicate a single recirculation, regions 2R* two-rolls regions. **S indicate stable structures, regions **U unstable structures. The NMF region is where no mean flow is possible because the recirculation is too slow for the size of the plume to be significantly convected, while in the NMF2 region no mean flow is possible because the plumes would be too thin to establish a large–scale flow. —··—, $(c/h)^2(k_f/k_w) = 1.28 \times 10^{-6}$ (for example gaseous helium/stainless steel with a sidewall thickness $c/h = 0.0025$); *, experiments by Niemela *et al.* (2000); ×, experiments by Chavanne *et al.* (2001).

In particular the experiment by Niemela *et al.* (2000) is contained in the 2RS and NMF regions for $Ra > 10^{11}$ while that by Chavanne *et al.* (2001) is at the boundary between the 1R* and 2R* regions for $Ra > 10^{10}$ and eventually is contained in the 1RS region: the fact that the high Rayleigh number parts of the two experiments belong to different regions of the phase diagram might explain the unreconciled difference in their heat transfer measurements. In addition, flow bimodality was observed for the highest values of Ra in the experiment by Chavanne *et al.* (2001) and by Roche *et al.* (2002) in the range $10^{10} < Ra < 10^{12}$ for an experiment whose Ra–Pr points are shifted about 3 decades to the left of the Ra-axis with respect to those of Chavanne *et al.* (2001). Although it might be coincidental, in both cases the Ra–Pr points are at the boundary between the 1R* and 2R* regions where the present model predicts the transition of the mean flow structure. As previously mentioned when discussing figure 4, for $Ra \leqslant Ra_C$ the single recirculation and the two-rolls configuration can be both supported by the system. This should be particularly true around $Ra = Ra_C$ where the strong flow unsteadiness can induce transitions between the two states. In this context it is possible that the Nusselt number attains two distinct values at the same Rayleigh number depending on the selected state. Further, if we allowed the system to accommodate a mean flow which is a linear combination of the two basic states, for a fixed Ra, any Nu value in between the two extrema would be in principle possible. This would certainly be a course for concern because it would imply that a Nusselt number value would only make sense if ensemble averaged over different runs at the same Ra (or over very long time intervals for a single experiment); on the other hand, at the moment there is no evidence of such a behaviour and therefore it should be considered only as a conjecture.

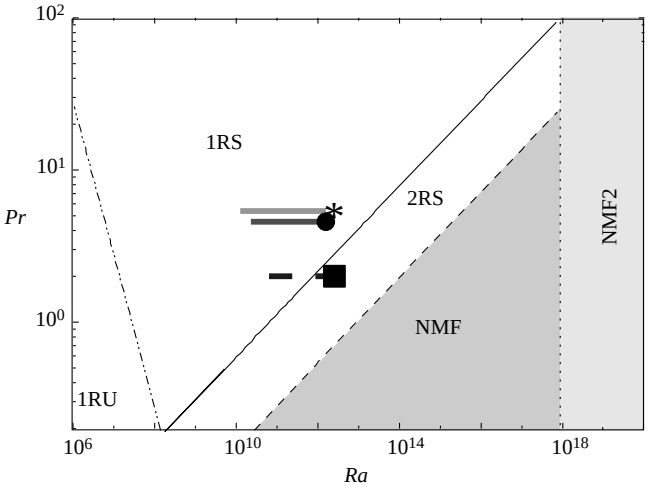

FIGURE 10. As figure 9 but —··—, $(c/h)^2(k_f/k_w) = 1.91 \times 10^{-4}$ (for example water/plexiglas with a sidewall thickness $c/h = 0.0125$), —— with *, experiments by Nikolaneko *et al.* (2004); —— with ●, experiments by Sun *et al.* (2005); - - - - ■, experiments by Chillà *et al.* (2004).

The water experiments have generally been performed at mean temperatures of $T = 50\,^{\circ}\mathrm{C}$ ($Pr = 4$–5) and in cells of heights $h = 0.4$–$0.5\,\mathrm{m}$, yielding $Ra \leqslant 5 \times 10^{11}$ and, according to figure 10, all contained in the 1 RS region. Only the work by Chillà *et al.* (2004) at a mean temperature of $T = 80\,^{\circ}\mathrm{C}$ ($Pr = 2$) and in a cell with $h = 1\,\mathrm{m}$ crosses a 2R* region with the transition occurring at $Ra = 8.5 \times 10^{11}$, which is very close to the value $Ra \approx 10^{12}$ reported by them for the onset of bimodal behaviour†.

The results for the low Prandtl number regime ($Pr \leqslant 0.1$) are reported in figure 11 with the separation between regions S and U drawn for the stainless steel and mercury combination. It can be seen that, to date, even the highest Rayleigh number experiments (Glazier *et al.* 1999) are all contained in the 1RU region which is consistent with the absence of flow bimodality reported for this fluid.

It is worth mentioning that the diagrams have been drawn only for $Pr \geqslant 0.5$ and $Pr \leqslant 0.1$ since in between these values none of the two $Nu(Ra, Pr)$ correlations used in this paper apply. In addition the Nu vs. Pr relation sketched in figure 3(b) in reality does not have a sharp edge around Pr_{th} but rather it presents a smooth transition between the increasing and constant branches. In this context, all the curvatures and details given by Grossmann & Lohse (2001) clearly become non-negligible, making the present model unrealistic.

A word of warning should also be given for the high Rayleigh number part of the phase diagram of figure 9 in connection with the ultimate regime proposed by Kraichnan (1962). In particular, in Kraichnan's scenario the boundary layer becomes turbulent because of the action of the largest eddies which are in fact the mean flow. Figure 9, however, indicates that for moderate Prandtl numbers at high enough Ra the system must enter the no-mean-flow state therefore suggesting that Kraichnan's regime is not accessible to the present $\Gamma = 1/2$ cell unless one has very high Prandtl

† The boundary between regions U and S of figure 10 does not apply to the experiment by Chillà *et al.* (2004) since in that case the sidewall was made of stainless steel and not of Plexiglas. Nevertheless this boundary is independent of the position of regions 1R and 2R and the above conclusions are not altered.

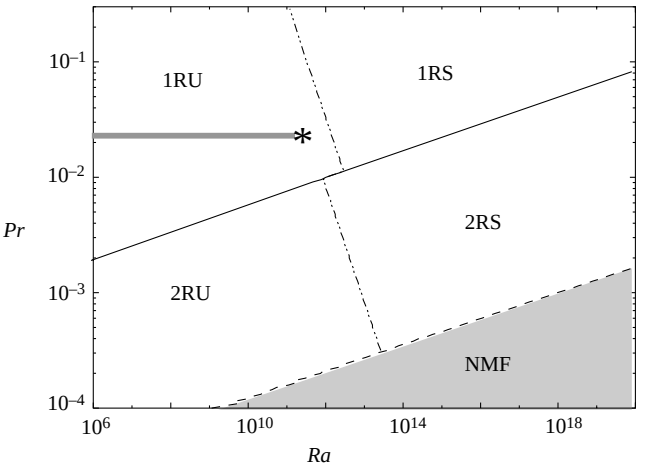

FIGURE 11. As figure 9 but —··—, $(c/h)^2(k_f/k_w) = 5.58 \times 10^{-6}$ (for example mercury/stainless steel with a sidewall thickness $c/h = 0.0025$); ——— with *, experiments by Glazier *et al.* (1999).

numbers in which case the regime reduces to that of Howard (1972) ($Nu \sim Ra^{1/3}$). On the other hand at moderate Pr when a large-scale flow is absent the thermal boundary layers at the upper and lower plates are not connected and, according to Malkus (1954) this should again give $Nu \sim Ra^{1/3}$. More specifically, as suggested by one of the referees, the line separating regions 2RS from NMF in figure 9 is essentially indistinguishable from the various lines in the Ra–Pr space for the ratio of the thermal and viscous boundary layer thicknesses equal to unity (see figure 11 of Niemela & Sreenivasan 2003), a necessary pre-condition for Kraichnan's regime to exist. Indirect evidence for the above arguments is given by the experiment of Niemela *et al.* (2000) who, having excluded the non-Boussinesq points and having corrected the remaining data for the sidewall and plate effects, deduced the relation $Nu = 0.088Ra^{0.32}$ (J. Niemela, personal communication) which is quite close to $Nu \sim Ra^{1/3}$. On the other hand, Roche *et al.* (2001) obtained some evidence of Kraichnan's regime by using non-smooth plates with grooves smaller than the thermal boundary layer thickness. In this case the boundary layers could be made turbulent with the help of the surface roughness and the new regime could be attained before crossing the 2RS–NMF boundary.

It should be noted that critical bifurcations induced by a particular value of the cell aspect ratio Γ are not a peculiarity of the present problem only. In fact Charlson & Sani (1971) reported an analogous phenomenon at the onset of convection; in particular they observed that for an aspect ratio smaller than $\gamma = 0.61$ and $\gamma = 0.81$, respectively for conducting and insulating sidewalls, the structure of the large-scale flow breaks the rotational symmetry (axisymmetric flow) to form a large asymmetric recirculation completely filling the cell. The analogy, however, should not be pushed too far since in the paper by Charlson & Sani (1971) the aspect ratio is defined with the radius of the cylinder $\gamma = R/h$ while in the present paper it is defined with the diameter $\Gamma = d/h$. This implies that the critical value $\gamma = 0.81$ corresponds to $\Gamma = 1.62$ (as directly verified by Oresta *et al.* 2005) which is not close to the present value $\Gamma = 0.5$.

Before concluding this paper we wish to stress that the various boundaries between the regions should be considered only as indicative since several numerical prefactors

could be used to tune the model. For example the ascending velocity of the side currents could be only a fraction (possibly *Pr*-dependent) of the free-fall velocity and their thickness a multiple of δ_θ. Similarly, the $Nu(Ra, Pr)$ relations could have different exponents and prefactors and the thresholds for the relations t_U/t_f and t_w/t_f could be adjusted instead of being strictly equal to one. In this study, however, we have deliberately decided not to use tunable constants in order to check if the raw arguments were able to capture the essential flow physics; the fact that the simplest version of the model agrees with the published literature seems to confirm our expectations.

The paper was conceived after presenting a paper at the 'High Rayleigh number convection Workshop' held on March 2005 at the JNCASR in Bangalore (India) and the authors are grateful to all the participants. Particular thanks go to A. B. Puthenveettil for his comments and suggestions. Thanks also to Professor J. Niemela and Drs F. Chillá and P. Roche for providing some experimental data and suggestions. The paper was prepared with the financial support of CEMeC of Politecnico di Bari.

REFERENCES

Ahlers, G. 2001 Effect of sidewall conductance on heat-transport measurements for turbulent Rayleigh–Bénard convection. *Phys. Rev.* E **6302**(2), 5303 U7–U9.

Araujo, F. F., Grossmann, S. & Lohse, D. 2005 Wind reversals in turbulent Rayleigh–Benard convection. *Phys. Rev. Lett.* **95**, 084502.

Brown, E., Nikolaenko, A. & Ahlers, G. 2005*a* Reorientation of the large-scale circulation in turbulent Rayleigh–Bénard convection. *Phys. Rev. Let.* (submitted).

Brown, E., Nikolaenko, A., Funfschilling, D. & Ahlers, G. 2005*b* Heat transport by turbulent Rayleigh–Bénard convection: effect of finite top and bottom plate conductivity. *Phys. Fluids* (Submitted).

Chavanne, X., Chillà, F., Chabaud, B., Castaing, B. & Hebral, B. 2001 Turbulent Rayleigh-Bénard convection in gaseous and liquid He. *Phys. Fluids* **13**, 1300–1320.

Charlson, G. S. & Sani, R. L. 1971 On thermoconvective instability in a bounded cylindrical fluid layer. *Intl J. Heat Mass Transfer* **14**, 2157–2160.

Chillà, F., Rastello, M., Chaumat, S. & Castaing, B. 2004 Long relaxation times and tilt sensitivity in Rayleigh Bénard turbulence. *Eur. Phys. J.* B **40**, 223–227

Cioni, S., Ciliberto, S. & Sommeria, J. 1997 Strongly turbulent Rayleigh-Bénard convection in mercury: comparison with results at moderate Prandtl number. *J. Fluid Mech.* **335**, 111–140.

Glazier, J. A., Segawa, T., Naert, A. & Sano, M. 1999 Evidence against ultra hard thermal turbulence at very high Rayleigh numbers. *Nature* **398**, 307–310.

Grossmann, S. & Lohse, D. 2001 Thermal convection for large Prandtl numbers. *Phys. Rev. Lett.* **86**(15), 3316–3319.

Grossmann, S. & Lohse, D. 2002 Prandtl and Rayleigh number dependence of the Reynolds number in turbulent thermal convection. *Phys. Rev.* E **66**, 016305-1–016305-6.

Grötzbach, G. 1983 Spatial resolution requirements for direct numerical simulation of the Rayleigh-Bénard convection. *J. Comput. Phys.* **49**, 241–264.

Horanyi, S., Krebs, L. & Müller, U. 1999 Turbulent Rayleigh–Bénard convection in low Prandtl number fluids. *Intl J. Heat Mass Transfer* **42**(21), 3983–4003

Howard, L. N. 1972 Bounds on flow quantities. *Annu. Rev. Fluid Mech.* **4**, 473–494.

Kraichnan, R. H. 1962 Turbulent thermal convection at arbitrary Prandtl number. *Phys. Fluids* **5**, 1374–1389.

Malkus, M. V. R. 1954 Heat transport and spectrum of thermal turbulence. *Proc. R. Soc. Lond.* A **225**, 196.

Monin, A. S. & Yaglom, A. M. 1975 *Statistical Fluid Mechanics*, vol. 2, MIT Press.

Niemela, J. J., Skrbek., L., Sreenivasan, R. R. & Donnelly, R. J. 2001 The wind in confined thermal convection. *J. Fluid Mech.* **449**, 169–178.

Niemela, J. J., Skrbek, L., Sreenivasan, K. R. & Donnelly, R. J. 2000 Turbulent convection at very high Rayleigh numbers. *Nature* **404**, 837–841.

Niemela, J. J. & Sreenivasan, K. R. 2003 Confined turbulent convection. *J. Fluid Mech.* **481**, 355–384.

Nikolaenko, A., Brown, E., Funfschilling, D. & Ahlers, G. 2005 Heat transport by turbulent Rayleigh–Bénard convection in cylindrical cells with aspect ratio one and less. *J. Fluid Mech.* **523**, 251–260.

Oresta, P., Stringano, G. & Verzicco, R. 2005 Transitional regimes and rotation effects in Rayleigh–Bénard convection in a slender cylindrical cell. *Eur. J. Mech.* B *Fluids* (Submitted).

Pope, S. B. 2000 *Turbulent Flows*. Cambridge University Press.

Puthenveettil, B. A. & Arakery, J. I. H. 2005 Plume structure in high Rayleigh number convection. *J. Fluid Mech.* **542**, 217–250.

Qiu X.-L. & Tong, P. 2001 Large-scale velocity structures in turbulent thermal convection. *Phys. Rev.* E **64**, 036304.

Roche, P. E., Castaing, B., Chabaud, B. & Hebral, B. 2002 Prandtl and Rayleigh numbers dependences in Rayleigh–Bènard convection. *Europhys. Lett*. **58**, 693–698.

Roche, P. E., Castaing, B., Chabaud, B. & Hebral, B. 2004 Heat transfer in turbulent Rayleigh–Bénard convection below the ultimate regime. *J. Low Temp. Phys.* **134**, 1011–1042.

Roche, P. E., Castaing, B., Chabaud, B., Hebral, B. & Sommeria, J. 2001*a* Side wall effects in Rayleigh–Benard experiments. *Eur. Phys. J.* B **24**, 405–408.

Roche, P. E., Castaing, B., Chabaud, B., Hebral, B. & Sommeria, J. 2001*b* Observation of the $1/2$ power law in Ranyleigh–Bénard convection. *Phys. Rev.* E **63**, 045303.

Rossby, H. T. 1969 A study of the Bénard convection with and without rotation. *J. Fluid Mech.* **36**, 309–335.

Sreenivasan, K. R., Bershadskii, A. & Niemela, J. J. 2002 Mean wind and its reversals in thermal convection. *Phys. Rev.* E **65**, 056306.

Sun, C., Xi, H. D. & Xia, K. Q. 2005 Azimuthal symmetry, flow dynamics and heat flux in turbulent thermal convection in a cylinder with aspect ratio one–half. *Phys. Rev. Lett*. (Submitted).

Verzicco, R. 2002 Side wall finite conductivity effects in confined turbulent thermal convection. *J. Fluid Mech.* **473**, 201–210.

Verzicco, R. & Camussi, R. 1999 Prandtl number effects in convective turbulence. *J. Fluid Mech.* **383**, 55–73.

Verzicco, R. & Camussi, R. 2003 Numerical experiments on strongly turbulent thermal convection in a slender cylindrical cell. *J. Fluid Mech.* **477**, 19–49.

Wu, X. Z. & Libchaber A. 1992 Scaling relations in thermal turbulence: The aspect-ratio dependence. *Phys. Rev.* A **45**, 842–845.